Experimental and numerical study of a second-order transition in the behavior of confined self-propelled particles

E. Barone
Universidad de Buenos Aires, Facultad de Ciencias Exactas y Naturales, Departamento de Física, Ciudad Universitaria, 1428 C. A. de Buenos Aires, Argentina

G. A. Patterson*
Instituto Tecnológico de Buenos Aires (ITBA), CONICET, Iguazú 341, 1437 C. A. de Buenos Aires, Argentina

(Received 28 November 2023; revised 18 March 2024; accepted 19 April 2024; published 29 May 2024)

In this paper, we conduct experimental investigations on the behavior of confined self-propelled particles within a circular arena, employing small commercial robots capable of locomotion, communication, and information processing. These robots execute circular trajectories, which can be clockwise or counterclockwise, based on two internal states. Using a majority-based stochastic decision algorithm, each robot can reverse its direction based on the states of two neighboring robots. By manipulating a control parameter governing the interaction, the system exhibits a transition from a state where all robots rotate randomly to one where they rotate uniformly in the same direction. Moreover, this transition significantly impacts the trajectories of the robots. To extend our findings to larger systems, we introduce a mathematical model enabling characterization of the order transition type and the resulting trajectories. Our results reveal a second-order transition from active Brownian to chiral motion.

DOI: 10.1103/PhysRevE.109.054609

I. INTRODUCTION

Active matter comprises systems of particles that consume energy to propel themselves or perform work [1,2]. One of the possible characteristics that these systems may exhibit is random behavior, exemplified by the trajectories of particles. These disturbances may be caused by environmental influences, internal stochastic processes related to the locomotion mechanism, or even decision-making arising from social interactions [3]. An active Brownian particle (ABP) is a type of particle model that describes the diffusive behavior, similar to that observed in some living organisms, and is characterized by the random change in the orientation of motion. This trait is adopted by various living beings as a strategy for environmental exploration, either to seek food or to distance themselves from potential threats [4–6]. One type of active particle that has received much attention in recent years is chiral active particles (CAPs). Chirality is not only a property of the geometry of objects but also of the trajectories that self-propelled particles undertake when the symmetry of the direction of motion is broken. There are various examples in nature of particles exhibiting chiral behavior. For instance, *E. coli* bacteria [7,8] and spermatozoa [9,10] exhibit chiral behavior when moving near a glass surface. There are also artificial systems, such as microswimmers, where the specific geometry of the particles generates chiral trajectories [11].

The simplest model to describe the behavior of a chiral active particle is based on specifying a translational velocity and an angular rotation [12]. Based on this definition, many studies have focused on exploring repulsion interactions [13,14], polar alignments [15,16], and synchronization [16,17]. Furthermore, there are studies that have investigated how the parameters governing the reorientation of particles determine the type of emerging trajectory of a particle confined in a channel [18].

The confinement of particles has been observed to enhance emergent behavior in nature, primarily due to interactions with the walls [19–21]. In particular, in the case of chiral particles, interactions with walls and obstacles produce currents biased by the polarity of rotation [22–24]. This phenomenon has inspired the design of containers that can organize and extract particles with specific polarity [25,26]. Previous studies have mainly focused on particles that interact through contact. The objective of this paper is to characterize the self-organized behavior of a system of particles that exhibit chiral behavior but modify their polarity through medium-range interactions. We investigate an experimental system of confined particles that can be programed to execute circular motion, communicate with neighbors, and process received information. While earlier works considered interactions aimed at aligning the direction of motion [27–29], in this paper, a majority-based stochastic interaction governs the rotation direction of the particles. The experiments were conducted using a commercial robot named Kilobot [30]. This type of agent has been employed to investigate various phenomena such as collective transport [31], pattern formation [32,33], morphogenesis [34], decision-making [35], food searching [36], chiral behavior induced by an external field [37], and decentralized learning [38].

The paper is organized as follows: In Sec. II, we first characterize the single Kilobot and then present experimental

*gpatters@itba.edu.ar

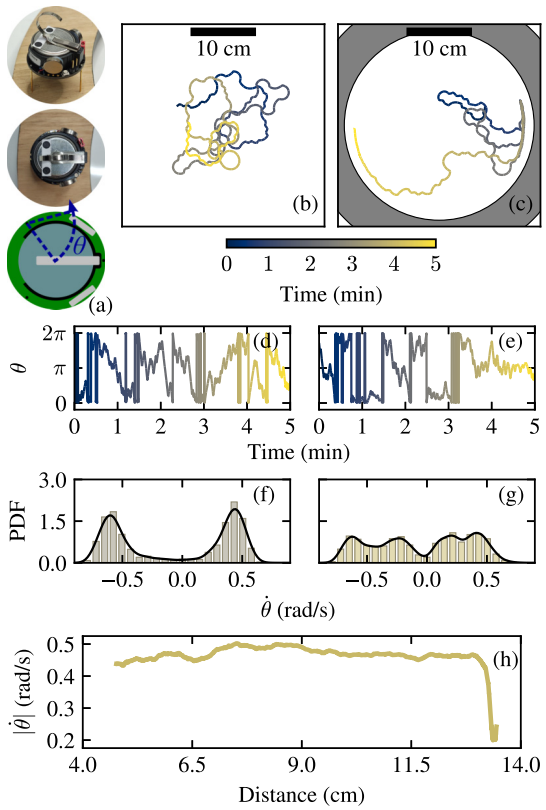

FIG. 1. (a) Photographs of the Kilobot showing the labels used for tracking and an illustration demonstrating counterclockwise rotation around the rear left leg. Five-minute trajectories of (b) an isolated robot and (c) a confined robot, with their respective orientations in (d) and (e). The color code represents time. Probability distributions of the angular velocity magnitude: (f) for the isolated robot and (g) for the confined robot. The black line represents the estimation using a Gaussian kernel function. (h) Average angular velocity as a function of distance from the center of the arena.

results demonstrating a shift in the system's behavior by varying a control parameter in the decision-making mechanism. In Sec. III, we introduce a mathematical model for the robots, enabling numerous simulations to characterize the scaling behavior and emerging trajectories, as well as analyzing the role of arena boundaries in the particle density. Finally, in Sec. IV, we discuss our conclusions.

II. EXPERIMENTAL RESULTS

A. Kilobot behavior and characterization

The Kilobots are 3.3 cm of diameter, 3.4 cm tall, and stand on three legs: one front and two rear. Each robot features two vibrators which are controlled independently by an internal microprocessor and allows the robot to rotate in one direction or the other around one of its rear legs [Fig. 1(a)]. Counterclockwise turns are made around the left leg, while clockwise turns are made around the right leg. As shown in the figure, we attached two circular markers on the robots to measure their absolute orientation and direction of rotation. Moreover, the robots have the ability to communicate with others within a distance of approximately 10 cm [30]. They can transmit information, such as the current rotation direction, at a rate of two messages per second. The robots have implemented a protocol that optimizes communication by reducing possible message collisions. Reception is isotropic, allowing messages to be received regardless of orientation within the communication distance. This communication, which operates unidirectionally, enables the microprocessor to update internal variables or robot motion based on the received information.

The motion of each robot was generated by clockwise or counterclockwise rotations. The direction of rotation was determined by an internal variable σ_i, which took a value of 1 for clockwise or -1 for counterclockwise. Each robot updated the value of σ_i with a period $T = 1$ s following the stochastic rule:

$$\begin{aligned} \sigma_i &\leftarrow -\sigma_i\ , \text{ with probability 1 if } \Phi_i < 0, \\ \sigma_i &\leftarrow -\sigma_i\ , \text{ with probability } p \text{ if } \Phi_i \geqslant 0, \\ \sigma_i &\leftarrow \sigma_i\ , \text{ with probability } 1-p \text{ if } \Phi_i \geqslant 0, \end{aligned} \tag{1}$$

where $\Phi_i = \sigma_i \sum_{j=1}^{M} \sigma_j$. M is the number of random messages considered out of all those received by robot i in each period T. We arbitrarily chose $M = 2$, so Φ_i could take values of -2, 0, or 2. While $\Phi_i = -2$ implies that robot i rotates in the opposite direction to the other two robots involved in the interaction, $\Phi_i = 2$ determines that all three robots rotate in the same direction. In the case of $\Phi_i = 0$, robot i has the same direction of rotation as one of the other robots, and it is considered to have the direction of the majority. The rule states that if the direction is opposite to the majority, with probability 1, the new rotation state will follow the majority. On the other hand, if the robot rotates in the same direction as the majority, then, with probability p, it inversely changes its rotation direction. In the case where no messages have been received during period T, the robot updates its rotation state randomly.

First, we analyzed the behavior of a single robot in the absence and presence of a confining arena. For the first case, we placed the robot on a white melamine board. For the second case, we further restricted the robot's motion with a circular arena of 15 cm radius. When not interacting with other agents, the Kilobot moved by performing random turns. The trajectories were recorded by an overhead video camera at a rate of 20 FPS. Figures 1(b) and 1(c) show trajectories of 5 min for the isolated and confined cases, respectively. It can be observed that the enclosure affects the robot's random trajectory, particularly showing periods where the Kilobot adheres to the container wall. Figures 1(d) and 1(e) show the particle's orientation over time. In the isolated case, the orientation evolves randomly. However, in the presence of the arena, there are periods of persistent orientation, indicated by constant values of θ in Fig. 1(e), corresponding to when the robot is in contact with the wall. We also analyzed the distributions of angular velocity. In the case of the isolated robot [Fig. 1(f)], the distribution is bimodal, describing counterclockwise and clockwise rotation speeds. On the other hand, in the case of the constrained robot [Fig. 1(g)], the distribution also shows probabilities of lower-intensity rotation speeds, which are consequences of the interaction with the walls. This

FIG. 2. Experimental setup. 20 Kilobots were positioned within a circular arena with a radius of 15 cm.

can be further confirmed by observing Fig. 1(h), which shows the angular velocity magnitude as a function of the distance to the center of the arena. Additionally, Fig. 1(f) highlights an asymmetry in the Kilobot motion, where the angular velocity shifts towards negative values, indicating a tendency to rotate clockwise. These individual differences are specific to each robot and could be exploited to achieve better performance in collective behaviors [39].

B. Collective behavior

Then, we placed 20 robots inside the arena whose trajectories were recorded at a rate of 1 FPS (Fig. 2). We studied the emergent behavior of the system as a function of the control parameter p. For this, we chose eight probability values in the range $p = [0.0 - 0.2]$, and for each of these, we let the system evolve for 60 min from random initial conditions (both spatial location and rotation state). Using image analysis, we were able to ascertain σ_i for every robot within each frame, enabling us to quantify the system's overall state by employing a conventional order parameter defined as

$$s(t) = \frac{1}{N}\sum_{i=1}^{N}\sigma_i(t), \tag{2}$$

where $s(t) = 1$ indicates that all robots rotate clockwise, $s(t) = -1$ counterclockwise, and $s(t) \approx 0$ suggests a balance between the two directions of rotation.

Figures 3(a)–3(f) present results for $p = 0.02$, 0.08, and 0.20. It can be observed that in the case of the lowest p [Fig. 3(a)], the system becomes completely ordered, showing some fluctuations due to the low probability of changing the rotation direction (Movie A in the Supplemental Material [40]). In the case of the highest p [Fig. 3(c)], the order parameter exhibits random behavior (Movie C in the Supplemental Material [40]). Finally, an intermediate value of p [Fig. 3(b)] shows that the order parameter fluctuates between the two possible ordered states (Movie B in the Supplemental Material [40]). Furthermore, analyzing the individual trajectories of

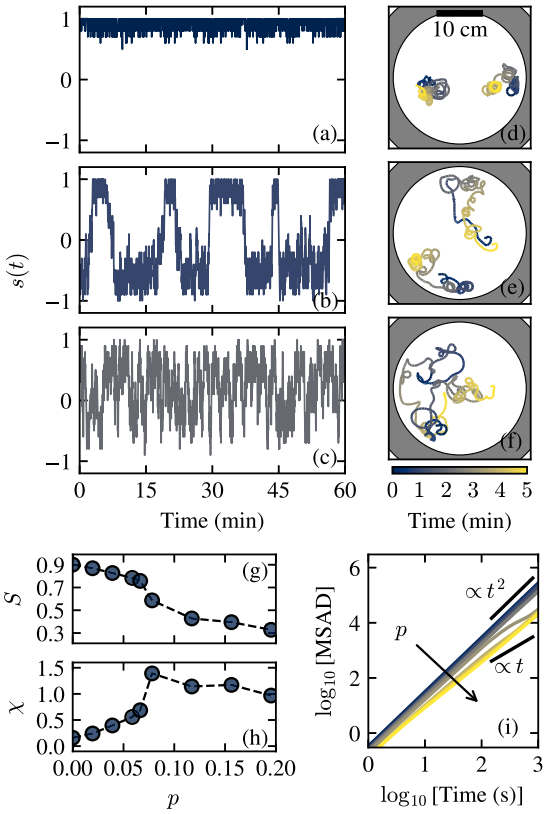

FIG. 3. Experimental results with 20 Kilobots. (a)–(c) Temporal evolution of the order parameter for $p = 0.02$, 0.08, and 0.20, respectively. (d)–(f) Trajectories performed by two robots during 5 min for the same values of p mentioned before. (g)–(h) Stationary average of the order parameter and susceptibility as a function of p. (i) Mean-squared angular displacement for different values of p. The arrow indicates the direction of increasing p, and the black lines show data trend.

the particles, it was observed that they undergo a noticeable change in behavior. While for small values of p [Fig. 3(d)], the trajectories were mostly circular and localized—resembling the behavior of CAPs—increasing this parameter caused the trajectories to cover a larger area in the same time interval with a less defined structure, similar to that of ABPs [Fig. 3(e) and 3(f)].

Then, for each value of p, we calculate $S = \langle|s(t)|\rangle$ and $\chi = N(\langle|s(t)|^2\rangle - \langle|s(t)|\rangle^2)$, the temporal average of the order parameter and the susceptibility, respectively. S measures the order state throughout the experiment: a value close to 0 implies disorder in the rotation directions, while a value close to 1 indicates an ordered system regardless of the direction. The susceptibility measures the fluctuations of S during the experiment. Results are shown in Figs. 3(g) and 3(h), where a monotonic relationship between the order parameter and the value of p can be observed. Additionally, a change in concavity is noticeable between the values of $p = 0.05$ and $p = 0.10$, along with a maximum value of susceptibility in the same interval. These findings are consistent with an order transition that we will characterize in the following section. We also analyzed how the parameter p influences the trajectories performed by the robots. For this, we calculated

the mean squared angular displacement (MSAD) given by $\mathrm{MSAD} = \langle \Delta\theta(t) \rangle^2$, where the brackets denote the average over all particles. Figure 3(i) shows the results we obtained for the different values of p. We analyzed the MSAD results on a log-log scale, where a temporal evolution with a slope of 2 indicates circular trajectories (CAP). On the other hand, a slope of 1 implies that the particle orientations and their trajectories follow symmetric diffusive behavior (ABP). The results show that at low values of p, the particles exhibit chiral behavior. As p increases, the MSAD deviates from ballistic behavior towards a diffusive one. However, it does not reach a slope of 1 due to the asymmetry in the angular velocity of the robots, as described in Figs. 1(f) and 1(g).

III. NUMERICAL RESULTS

To delve deeper into the study of the system, a model was proposed that incorporates the main experimental features: polar circular particles that move by rotating in both directions and can exchange information with neighbors to update their motion state. The particles are characterized by their position $\boldsymbol{r}$, orientation $\boldsymbol{n} = (\cos\theta, \sin\theta)$, and motion state σ_i. The evolutions of the position and orientation are given by

$$\dot{\boldsymbol{r}}_i = v_0\, \boldsymbol{n} + \boldsymbol{f}_{ij}, \tag{3}$$

$$\dot{\theta} = -\sigma_i(t)\frac{|\dot{\boldsymbol{r}}_i|}{R_p} + \eta, \tag{4}$$

$$\boldsymbol{f}_{ij} = -\kappa\epsilon\hat{\rho}_{ij}, \tag{5}$$

where v_0 is the translational velocity of the particle, R_p is the turning radius, and η is an uncorrelated, zero-mean Gaussian perturbation with amplitude D, accounting for the robot's vibration. f_{ij} is the interaction force with other particles and the arena. This is a repulsive force depending on the overlap distance ϵ between the two involved objects, an intensity constant κ, and the normal contact direction given by $\hat{\rho}_{ij} = \frac{\boldsymbol{r}_j - \boldsymbol{r}_i}{|\boldsymbol{r}_j - \boldsymbol{r}_i|}$. A free particle will move with a velocity v_0, describing, on average, circular trajectories with a turning radius of R_p and a direction given by $\sigma_i(t)$. This is motivated by the experimental system where the robot's rotations are around one of its rear legs. The update of the state σ_i followed the same rules as in the experimental system: for each particle, Φ_i was calculated with a period T, considering $M = 2$ particles within a radius of 10 cm. The parameters were chosen as follows: the turning radius was fixed as the Kilobot radius, $R_p = 1.65$ cm. For the translational velocity, we took an approximate rotation value of $\theta = 0.5$ rad/s [Fig. 1(f)] to calculate $v_0 = |\dot{\theta}|R_p = 0.825$ cm/s. The constant κ was chosen so a 1% overlap with another object of the particle's radius produces a repulsive force of equal intensity to propulsion, i.e., $v_0/\kappa = R_p/100$. For the perturbation, we used a value of $D = 0.05$, sufficient to break deadlock situations that the robots resolve with their vibrations [41].

We simulated the equations using the Euler-Maruyama algorithm with an integration step of $dt = 10^{-2}$ s and a simulation length of 10^5 s. We varied the number of agents in the range $N = [20 - 2000]$ and the confinement radius $R = \sqrt{\frac{N}{\pi\rho_0}}$ to fix the density at the value $\rho_0 = 0.028$ cm^{-2} used in the experiment. Figure 4 presents numerical results,

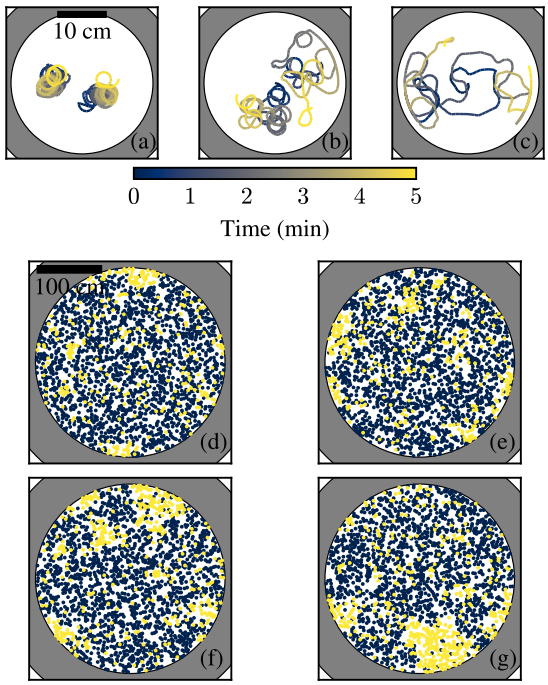

FIG. 4. Numerical results. (a)–(c) Trajectories performed by two particles during 5 min for $N = 20$ and $p = 0.02$, 0.08, and 0.20, respectively. (d)–(g) Snapshots of system configurations at different times for $N = 2000$ and $p = 0.07$. The color of the particles indicates the direction of rotation: yellow for counterclockwise and blue for clockwise. The size of the particles has been enlarged for better visualization. The parameters used in the simulation were $v_0 = 0.825$ cm/s, $R_P = 1.65$ cm, $D = 0.05$, and $\kappa = 50$ 1/s.

specifically, individual trajectories of some particles for the cases of $p = 0.02$, 0.08, and 0.20 with $N = 20$. Comparing with the results shown in Figs. 3(d)–3(f), we find a qualitative agreement of the particle trajectories under different regimes. Additionally, we observed that in larger systems, the system exhibits spatial inhomogeneities. In Figs. 4(d)–4(g), snapshots of the system's evolution are shown, where the inhomogeneities represented by clusters of different sizes and spatial locations can be observed for a value of $p = 0.07$. These inhomogeneities are characteristic of systems undergoing second-order phase transitions and are found near their critical point.

In Fig. 5, the results of the order parameter S, susceptibility χ, and the reduced fourth-order cumulant of Binder defined as $U = 1 - \frac{\langle s(t)^4 \rangle}{3\langle s(t)^2 \rangle^2}$ are shown. The results are the average of 100 independent realizations. The order parameter [Fig. 5(a)] shows that, for this particular density, when the value of p is reduced below a critical value, there is a transition from a disordered phase to an ordered one. Additionally, it can be observed that the transition is more pronounced when considering larger systems. Figure 5(b) shows the dependence of susceptibility on p and N. The curves exhibit peak values whose location depends on N. As the system size increases, the maximum value of χ is located at smaller values $p_\chi(N)$ and appears to saturate at a value p_c. On the other hand, Fig. 5(c) shows the curves of the Binder parameter $U(p)$. It can be observed that two curves corresponding to sizes N_i and

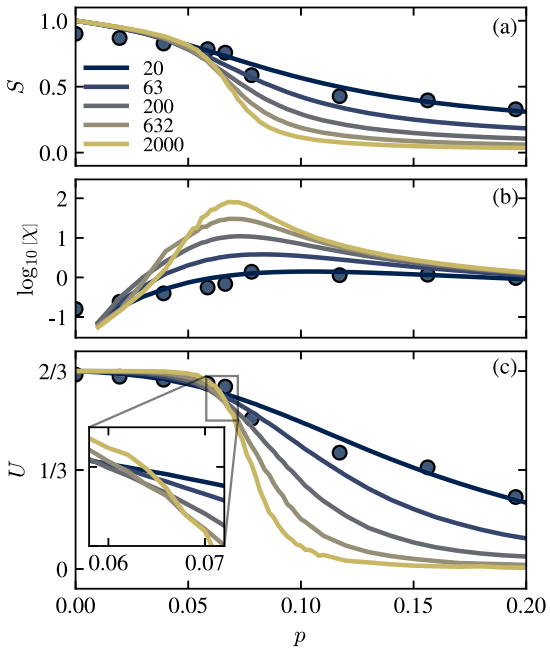

FIG. 5. Numerical results. (a) Order parameter, (b) susceptibility, and (c) Binder coefficient as a function of p. The solid lines depict results for five system sizes, and the symbols represent experimental data for $N = 20$. The inset in (c) provides a detailed view of the intersection between the different curves.

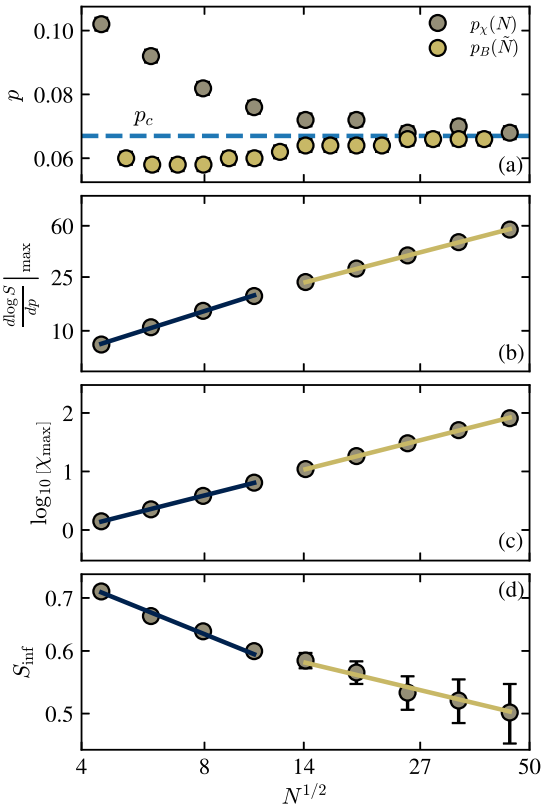

FIG. 6. (a) Positions of the maxima of the susceptibility and the intersections of the Binder parameter as a function of the system size ($N^{1/2}$) in a semilog scale. (b) Maximum value of the derivative of the decimal logarithm ($\log_{10}$) of the order parameter. (c) Maximum values of the susceptibility. (d) Value of the order parameter evaluated at the inflection point. The solid lines are fits made in two ranges of system size. (b)–(d) are in log-log scale.

N_j intersect at a probability value $p_B(N_i, N_j)$ and, moreover, the location of the intersection appears to saturate at p_c when observing larger systems. The absence of negative values of the Binder parameter indicates that the order transition is consistent with a second-order one. Experimental results are also presented in the figure to demonstrate the excellent agreement with the numerical findings.

Figure 6(a) shows the values of p_χ and p_B as a function of the corresponding size. To describe the system's size, we used $N^{1/2}$, which, at constant density, is proportional to the arena radius R. In the case of p_B, we used an equivalent value of N defined as $\tilde{N} = \sqrt{N_i N_j}$. The results of $p_B(\tilde{N})$ show a variation greater than 10%, contrary to what the theory suggests, where all U curves should intersect at the critical value p_c. However, when considering larger systems, the two data sets converge to a critical value estimated at $p_c = 0.067(1)$. Next, to characterize the transition, we studied the numerical results through a finite-size scaling analysis and calculated the standard critical exponents: ν, γ, and β. For the first, we studied the scaling behavior of the maximum value of the derivative of the decimal logarithm of the order parameter, following a power-law of the form [42]

$$\left.\frac{d\log S}{dp}\right|_{\max} \propto N^{1/2\nu}. \tag{6}$$

In Fig. 6(b), we plotted the obtained values as a function of the system size on a log-log scale. We found that the data does not follow a linear trend across the entire range. Therefore, we performed two fits of Eq. (6): one for the lower values of the system size and another for the higher values. For the first one, the calibration led us to a value $\nu^L = 1.04(3)$, and for the second, we obtained $\nu^H = 1.27(1)$. The results show significant differences, indicating a change in the behavior of the correlation length with increasing system size.

Then, we study the relationship between the maximum susceptibility value $\chi_{\max}$ and the characteristic system size N. For this, the scaling law is expressed as follows:

$$\chi_{\max} \propto N^{\gamma/2\nu}. \tag{7}$$

Encouraged by the previous results, we also performed two fits of Eq. (7). In Fig. 6(c), the obtained results are shown. For the lower values, we obtained $(\gamma/\nu)^L = 1.77(2)$, while for the higher, the value was $(\gamma/\nu)^H = 1.76(1)$. In the case of susceptibility, we found that the results between both regions do not present significant differences and, moreover, the value γ/ν corresponds to that of the 2D Ising model.

Then, we investigate the scaling behavior of the order parameter at the inflection point $S_{\inf}$ in relation to $N^{1/2}$. This scaling behavior is described by the following power-law relationship:

$$S_{\inf} \propto N^{-\beta/2\nu}. \tag{8}$$

Figure 6(d) shows the obtained results. The inflection point of each curve was determined by finding the value of p corresponding to the maximum of the numerical derivative of S.

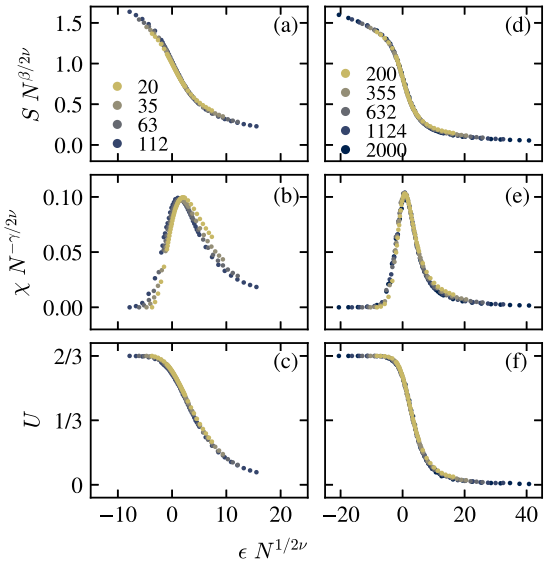

FIG. 7. Collapse of the data considering (a)–(c) the smaller sizes, and (d)–(f) the larger ones. The figures were plotted using $p_c = 0.067$ and the corresponding values of $\nu^{L,H}$, $(\gamma/\nu)^{L,H}$, and $(\beta/\nu)^{L,H}$ as indicated in the text.

We performed two fits again and obtained $(\beta/\nu)^L = 0.21(2)$ and $(\beta/\nu)^H = 0.123(8)$, respectively. The results differ significantly, and, similar to the susceptibility, in the higher range of sizes, the value of β/ν corresponds to that of the Ising model in 2D.

The finite-size scaling behavior can be verified by plotting $S\,N^{\beta/2\nu}$, $\chi\,N^{-\gamma/2\nu}$, and U as a function of $\epsilon\,N^{1/2\nu}$, where $\epsilon = p/p_c - 1$ and $p_c = 0.067$. In Figs. 7(a)–7(c), the collapse of the curves for the smaller sizes is shown. While the collapse seems relatively appropriate for the order and Binder parameters, a strong discrepancy is observed for the susceptibility. On the other hand, for the larger sizes [Figs. 7(d)–7(f)], the collapse of all three quantities is satisfactory. Furthermore, we found that the hyperscaling relation $2\beta/\nu + \gamma/\nu = 2$ holds in the higher range, resulting in 2.01(2), but it fails in the lower one, yielding 2.18(4).

Then, we characterized the trajectories of the particles as a function of p. To do this, we calculated the MSAD for $N = 2000$ to have a larger statistical ensemble. Figure 8(a) shows the results obtained for different p values. The findings indicate that, similar to the experimental observations, particles at low p values display chiral behavior. As p increases, the system transitions to a disordered phase, following Brownian trajectories. Unlike the experiments, the numerical results tend to exhibit a slope of 1 due to the symmetric angular velocity of the simulated particles. We quantified the transition from chiral to Browninan behavior by fitting the MSAD for $t > 100$ s using functions of the form t^α. In Fig. 8(b), we present the values of α obtained for each p. It can be observed that there is a change in the particle motion behavior upon crossing the critical value p_c: the phase transition from ordered to disordered state results in a transition from CAP to ABP behavior.

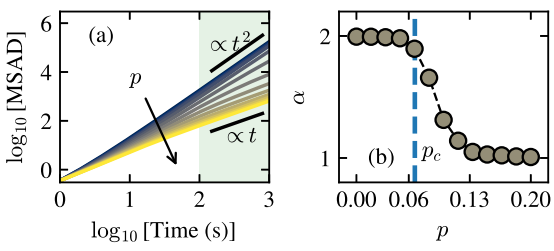

FIG. 8. (a) Mean-squared angular displacement for different values of p. The results correspond to the $N = 2000$ system. The arrow indicates the direction of increasing p. The black lines show data trend. The shaded region represents the set of data fitted by a function of the form t^α. (b) Values of α obtained from the previous fits. The vertical line indicates the estimated value of p_c from Fig. 6(a).

The system under study is a network in which connections between nodes vary over time because they depend on the motion of the agents. When an agent is at a distance greater than its communication range from its nearest neighbor, its behavior becomes random, introducing a disturbance in the global state of the system. To characterize how frequent this disturbance is, we estimated the probability per unit of time, P_d, that the distance to the nearest neighbor is greater than 10 cm, i.e., the probability that an agent has not received messages at each state update step. Figure 9(a) shows the results obtained for the experimental and numerical systems with $N = 20$ as a function of p. It can be observed that as p increases, the probability of not receiving messages grows in both systems. We can see that for values near the critical point, the probability is significantly higher than for lower p values. The greater variability in the experimental results is due to the smaller amount of data used for the estimation. Then, Figure 9(b) shows the numerical results of P_d as a function of N. We can observe that for higher p values, the probability decreases with increasing size until reaching values comparable to those of lower p values. It can be seen that for $N > 200$, the probability of the nearest neighbor being at a distance greater than 10 cm is practically uniform, and the randomness source due to the individual behavior of the agents is independent of p.

To understand the cause behind these differences in P_d, we characterized how the particles are distributed within the arena. For this, we divided the space into two regions—one bulk and the other surface—using a circle of radius $R_c = R - 2R_P$. Then, we calculated the density of bulk particles according to

$$\rho_B = \frac{N_B}{\pi R_c^2}, \tag{9}$$

where N_B is the number of particles located at a distance from the center of the arena less than R_c. We also calculated the density of particles on the surface using

$$\rho_S = \frac{N - N_B}{\pi\left(R^2 - R_c^2\right)}. \tag{10}$$

Figure 9(c) displays the relative density results for $N = 20$ for both the experimental and numerical systems. For this, we used the experimental density $\rho_0 = 0.028$ cm^{-2} as the reference value. A consistent trend is observed in both data sets: the bulk density decreases with increasing p, while the

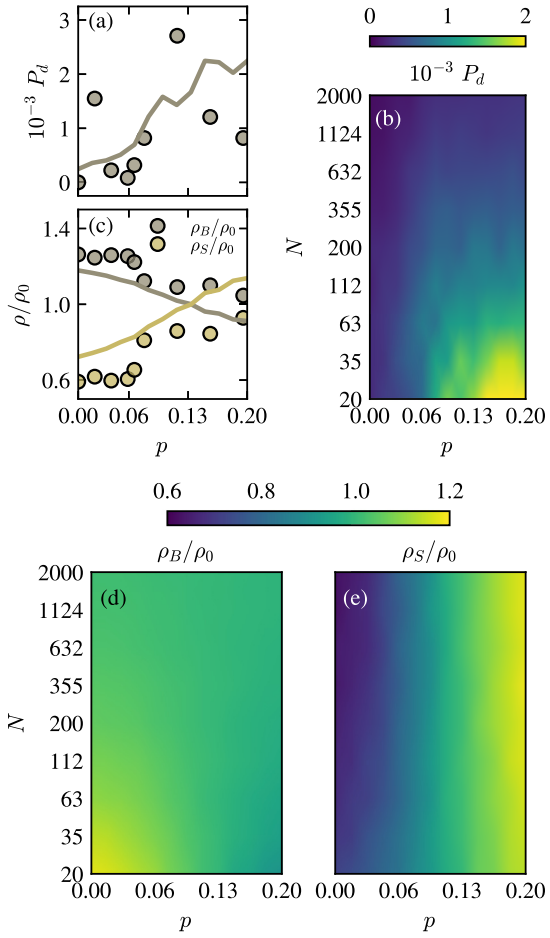

FIG. 9. (a) Probability of not receiving messages per unit time as a function of p for the experimental (symbol) and numerical systems (solid line), both with $N = 20$. (b) Same probability for the numerical system as a function of N. (c) Relative density as a function of p for $N = 20$, both for the bulk (ρ_B) and the surface (ρ_S). Points correspond to experimental results, and lines to numerical ones. Relative density of (d) bulk and (e) surface as a function of p and N.

surface density increases. This indicates a notable migration of particles toward the surface region. This decrease in particles within the arena's interior increases the likelihood of particles being outside the communication range of their neighbors [see Fig. 9(b)]. As N increases, the numerical results show that the bulk density becomes uniform across the entire range of p [Fig. 9(d)]. Subsequently, in Fig. 9(e), we present the results related to the density of particles near the surface for various N. It is evident across all the analyzed sizes that increasing p enhances the particle density at the surface. This outcome is expected due to the reduction in rotational speed that we observed in the previous characterization. This explains why the bulk density decreases at higher values of p, where the particles in the system behave like ABPs. Additionally, it is noteworthy that the number of agents present on the surface scales with $N^{1/2}$, while in the bulk it grows linearly with N. Consequently, the average bulk density tends to ρ_0 and P_d becomes uniform, regardless of p, as the system size increases. This analysis provides an explanation for the failure of the scaling in smaller systems: in those cases, the system's behavior is significantly influenced by the arena's presence. The accumulation of particles on the surface for higher p values alters the degree of communication between agents and introduces randomness in the behavior of isolated particles.

IV. CONCLUSION

In summary, we investigated the emergent behavior of an interacting particle system confined within a circular arena. For this purpose, we employed 20 commercially available robots known as Kilobots. These robots possess differential locomotion capabilities and can communicate with their neighbors. They were programed with two rotational motion states: one in the clockwise and the other in the counterclockwise direction. Using a stochastic interaction that considered the rotational states of two neighboring units, each robot had the ability to change its own rotational state. The interaction was mediated by a control parameter, where higher values led to a disordered and symmetric behavior, implying that robots rotated randomly in both directions. Upon reducing the parameter below a certain threshold, the system exhibited a symmetry breaking where all robots rotated in a uniform direction. Furthermore, we observed that as a consequence of this transition, the trajectories of the particles exhibited a noticeable change: below the threshold, they were circular, while above it they displayed random motion.

Then, we employed a mathematical model to extend the results to larger systems. This enabled us to characterize the transition of the system using the order parameter, susceptibility, and Binder parameter. We found that the results did not meet the scaling relation in the studied range. Consequently, we opted to conduct a finite-size analysis in two regions. The critical exponents determined for the smaller size region failed to satisfy the hyperscaling relationship and resulted in poor curve collapses, notably in the susceptibility. Conversely, within the larger size region, the exponents adhered to the hyperscaling relationship, and the curves displayed excellent collapse in scaling renormalization. An intriguing aspect of the critical exponents in the higher region is that both $\gamma/\nu = 1.76(1)$ and $\beta/\nu = 0.123(8)$ agree with those of the 2D Ising model. However, the value $\nu = 1.27(1)$ significantly differs. In addition, we found that the transition type corresponded to that of a second order.

We also studied the MSAD and confirmed what was observed in the experiments: the system's order transition is accompanied by a transition in the particles' trajectories. While in the disordered state, the particles exhibit diffusive trajectories characterized by an evolution like MSAD $\propto t$, in the ordered state, we found a relationship of the form MSAD $\propto t^2$, indicating chiral behavior.

Finally, we measured the probability per unit time, P_d, that an agent does not receive messages because it is at a distance greater than the communication range. We found that, both in the experimental and in the smaller numerical systems, P_d was affected by the control parameter p. In the case of larger systems, P_d is low and independent of p. Analyzing the bulk density distribution, we observed that for the smaller system sizes it is notably sensitive to the control parameter. This is

because for high values of p, the particles behave like ABPs and tend to accumulate at the boundaries of the arena, as shown in the calculation of the surface density. However, in the larger systems, the bulk density shows independence from the control parameter. This is attributed to the limitation on the number of particles that can reside on the surface, which scales proportionally with the system's radius, that is, $N^{1/2}$. This results in the failure of the scaling analysis for the smaller systems, as the dependence of the bulk density and P_d on the control parameter causes random disturbances in that size range.

The findings from this study hold significant implications in the field of swarm intelligence, wherein system functionalities often scale with the number of particles without requiring a redefinition of interaction types. Specifically, the behavior demonstrated by this system can be adopted as a search strategy, where the control parameter acts as the response to a environmental stimulus. Regarding future research directions, it would be valuable to investigate how the speed of particles influences emergent behavior. Evidence from self-propelled particle systems that engage in opinion exchange suggests that the critical point of the order transition is directly related to the particles' translational speed. Specifically, these systems exhibit a critical point at a perturbation value of zero under static conditions [43]. Further investigation into how the system responds to changes in interaction characteristics would be valuable. Recent studies with robots have demonstrated improved adaptability to changes when agents operate within a reduced communication range [44]. Therefore, exploring the impact of varying the number of interacting agents and the interaction radius could provide deeper insights into the system's behavior.

ACKNOWLEDGMENTS

This work was funded by project PICT No. 2019-00511 (Agencia Nacional de Promoción Científica y Tecnológica, Argentina). The authors extend special thanks to P. Balenzuela for his valuable comments and suggestions in the early stages of this work.

[1] S. Ramaswamy, Annu. Rev. Condens. Matter Phys. **1**, 323 (2010).
[2] E. Fodor and M. C. Marchetti, Physica A **504**, 106 (2018), Lecture Notes of the 14th International Summer School on Fundamental Problems in Statistical Physics.
[3] P. Romanczuk, M. Bär, W. Ebeling, B. Lindner, and L. Schimansky-Geier, Eur. Phys. J. Spec. Top. **202**, 1 (2012).
[4] Rotary motor, in *E. coli in Motion*, edited by H. C. Berg (Springer New York, New York, 2004), pp. 105–120.
[5] M. E. Cates, Rep. Prog. Phys. **75**, 042601 (2012).
[6] W. C. K. Poon, Proc. Intl. School Phys. Enrico Fermi **184**, 317 (2013).
[7] W. R. DiLuzio, L. Turner, M. Mayer, P. Garstecki, D. B. Weibel, H. C. Berg, and G. M. Whitesides, Nature (London) **435**, 1271 (2005).
[8] E. Lauga, W. R. DiLuzio, G. M. Whitesides, and H. A. Stone, Biophys. J. **90**, 400 (2006).
[9] I. H. Riedel, K. Kruse, and J. Howard, Science **309**, 300 (2005).
[10] B. M. Friedrich and F. Jülicher, Proc. Natl. Acad. Sci. USA **104**, 13256 (2007).
[11] F. Kümmel, B. ten Hagen, R. Wittkowski, I. Buttinoni, R. Eichhorn, G. Volpe, H. Löwen, and C. Bechinger, Phys. Rev. Lett. **110**, 198302 (2013).
[12] B. Liebchen and D. Levis, Europhys. Lett. **139**, 67001 (2022).
[13] M. E. Cates and J. Tailleur, Annu. Rev. Condens. Matter Phys. **6**, 219 (2015).
[14] E. Sesé-Sansa, D. Levis, and I. Pagonabarraga, J. Chem. Phys. **157**, 224905 (2022).
[15] B. Liebchen and D. Levis, Phys. Rev. Lett. **119**, 058002 (2017).
[16] B. Ventejou, H. Chaté, R. Montagne, and X.-q. Shi, Phys. Rev. Lett. **127**, 238001 (2021).
[17] D. Levis, I. Pagonabarraga, and B. Liebchen, Phys. Rev. Res. **1**, 023026 (2019).
[18] S. van Teeffelen and H. Löwen, Phys. Rev. E **78**, 020101(R) (2008).
[19] F. Peruani, J. Starruß, V. Jakovljevic, L. Søgaard-Andersen, A. Deutsch, and M. Bär, Phys. Rev. Lett. **108**, 098102 (2012).
[20] H. Wioland, F. G. Woodhouse, J. Dunkel, J. O. Kessler, and R. E. Goldstein, Phys. Rev. Lett. **110**, 268102 (2013).
[21] T. Ostapenko, F. J. Schwarzendahl, T. J. Böddeker, C. T. Kreis, J. Cammann, M. G. Mazza, and O. Bäumchen, Phys. Rev. Lett. **120**, 068002 (2018).
[22] B.-q. Ai, Sci. Rep. **6**, 18740 (2016).
[23] X. Yang, C. Ren, K. Cheng, and H. P. Zhang, Phys. Rev. E **101**, 022603 (2020).
[24] P. Liu, H. Zhu, Y. Zeng, G. Du, L. Ning, D. Wang, K. Chen, Y. Lu, N. Zheng, F. Ye, and M. Yang, Proc. Natl. Acad. Sci. USA **117**, 11901 (2020).
[25] T. Barois, J.-F. Boudet, J. S. Lintuvuori, and H. Kellay, Phys. Rev. Lett. **125**, 238003 (2020).
[26] W. Li, L. Li, Q. Shi, M. Yang, and N. Zheng, Powder Technol. **407**, 117671 (2022).
[27] F. Ginelli, Eur. Phys. J. Spec. Top. **225**, 2099 (2016).
[28] G. Baglietto and F. Vazquez, J. Stat. Mech.: Theory Exp. (2018) 033403.
[29] K. S. Olsen, L. Angheluta, and E. G. Flekkøy, Phys. Rev. Res. **4**, 043017 (2022).
[30] M. Rubenstein, C. Ahler, and R. Nagpal, Kilobot: A low cost scalable robot system for collective behaviors, *2012 IEEE International Conference on Robotics and Automation, Saint Paul, MN* (IEEE, Piscataway, NJ, 2012), pp. 3293–3298.
[31] M. Rubenstein, A. Cabrera, J. Werfel, G. Habibi, J. McLurkin, and R. Nagpal, Collective transport of complex objects by simple robots: Theory and experiments, in *12th International Conference on Autonomous Agents and Multiagent Systems 2013, AAMAS 2013*, Vol. 1 (IFAAMAS, 2013), pp. 47–54.
[32] M. Rubenstein, A. Cornejo, and R. Nagpal, Science **345**, 795 (2014).
[33] M. Gauci, R. Nagpal, and M. Rubenstein, Programmable self-disassembly for shape formation in large-scale robot collectives, in *Distributed Autonomous Robotic Systems: The 13th*

International Symposium, edited by R. Groß, A. Kolling, S. Berman, E. Frazzoli, A. Martinoli, F. Matsuno, and M. Gauci (Springer International Publishing, Cham, 2018), pp. 573–586.

[34] I. Slavkov, D. Carrillo-Zapata, N. Carranza, X. Diego, F. Jansson, J. Kaandorp, S. Hauert, and J. Sharpe, Sci. Robotics **3**, eaau9178 (2018).

[35] G. Valentini, E. Ferrante, H. Hamann, and M. Dorigo, Auton. Agent Multi-Agent Syst. **30**, 553 (2016).

[36] A. Font Llenas, M. S. Talamali, X. Xu, J. A. R. Marshall, and A. Reina, in *Swarm Intelligence*, edited by M. Dorigo, M. Birattari, C. Blum, A. L. Christensen, A. Reina, and V. Trianni (Springer International Publishing, Cham, 2018), pp. 135–149.

[37] G. A. Patterson, Phys. Rev. E **106**, 014615 (2022).

[38] M. Y. B. Zion, J. Fersula, N. Bredeche, and O. Dauchot, Sci. Robotics **8**, eabo6140 (2023).

[39] M. Raoufi, P. Romanczuk, and H. Hamann, Individuality in swarm robots with the case study of Kilobots: Noise, bug, or feature? in *Proceedings of the ALIFE 2023 Ghost in the Machine Proceedings of the 2023 Artificial Life Conference* (ASME, 2023), p. 35.

[40] See Supplemental Material at http://link.aps.org/supplemental/10.1103/PhysRevE.109.054609 for experimental videos of the system evolution for $p = 0.02$, 0.08, and 0.20.

[41] D. Helbing and P. Molnár, Phys. Rev. E **51**, 4282 (1995).

[42] L. G. López, D. H. Linares, and A. J. Ramirez-Pastor, Phys. Rev. E **80**, 040105(R) (2009).

[43] E. S. Loscar, G. Baglietto, and F. Vazquez, Phys. Rev. E **104**, 034111 (2021).

[44] M. S. Talamali, A. Saha, J. A. R. Marshall, and A. Reina, Sci. Robotics **6**, eabf1416 (2021).